The role of SP-B_{1-25} peptides in lung surfactant monolayers exposed to gold nanoparticles

Received 00th January 20xx,
Accepted 00th January 20xx

DOI: 10.1039/x0xx00000x

Sheikh I. Hossain[a], Neha S. Gandhi[b], Zak E. Hughes[c], Suvash C. Saha[a*]

Lung surfactant (LS) monolayers **that** continuously expand and compress **during** breathing cycles, act as the first line barrier for inhaled nanoparticles. It is known that nanoparticles which adsorb to the surface of the surfactant layer facilitate the rearrangement of lipids and peptides at various stages of the breathing cycle. However, the structural mechanisms for this ability of the lipid rearrangement are not yet fully understood. Coarse-grained molecular dynamics simulations are performed to investigate the role of **surfactant protein B** (SP-B) **segments (SP-B_{1-25})** in modulating the biophysical properties of the surfactant monolayer in the presence of polydisperse gold nanoparticles (AuNPs) at different concentrations. Herein, we observe that the AuNPs significantly alter the inherent structural and dynamical properties of the monolayer and its components in three different breathing states. When adsorbed into the monolayer, the AuNPs inhibit the ability of the monolayer to recover its surface tension and other properties. The presence of SP-B_{1-25} in the monolayer accelerates the diffusion of the monolayer phospholipids, contrarily to the role of AuNPs on phospholipid diffusion. Also, the AuNPs and the peptides in the monolayer significantly increase their agglomeration in the presence of one another. Overall, the simulations predict that the presence of polydisperse AuNPs hampers the stability and biophysical functions of the LS in contrast to the role of the peptide. This study provides a clear view of hydrophobic peptide role on the LS monolayer at the interface along with the interactions and the translocation of AuNPs that could have a significant impact to assess the NPs inhalation.

1. Introduction

A lung surfactant (LS) layer is responsible for the cycling of lung volume during the respiration process. It controls the surface tension at the air-water interface in alveoli to prevent alveolar collapse and reduce the work of breathing. The LS layer is a mixture of saturated and unsaturated phospholipids (PLs), and cholesterol, which combined make up 90 wt% of the LS. Small amounts (~10 wt%) of surfactant proteins (SP), both hydrophilic (e.g. SP-A, and SP-D) and hydrophobic (e.g. SP-B, and SP-C) are also found in the LS.[1] Hydrophobic surfactant monolayer associated proteins, SP-B/-C, and surfactant lipids, mainly dipalmitoylphosphatidylcholine (DPPC)**, unsaturated lipids, such as** 1-palmitoyl-2-oleoyl-sn-glycero-3-phosphoglycerol (POPG), and cholesterol **(neutral lipid)** form a stable monolayer at the air-water interface of the lung alveoli and, thus, stimulate the gas exchange process during breathing.[2] The LS monolayer components stabili**se** the monolayer, with the role of surfactant proteins being significant. For example, the surfactant peptide SP-B initiates folding of the LS by fluidizing the monolayer[3, 4]. During the LS monolayer compression (during exhalation), the surface tension at the interface is reduced to ~0 mN/m from the equilibrium surface tension ~20-25 mN/m, achieved upon membrane expansion (inhalation).[5] The interfacial surface tension of the LS monolayer is responsible for determining much of the structural, dynamical, and biophysical characteristics of the surfactant layer.[6] As such, it is essential to understand the changes inhaled species make to the structural and dynamical properties of the monolayer as these will, in turn, affect the biophysical properties of LS monolayer.

Fine and ultrafine particles ($PM_{2.5}$<2.5 μm and $PM_{0.1}$<100 nm) at high concentrations pose the greatest risk to human health as they rapidly and easily enter into deep area of the respiratory system and cause lung dysfunction.[7] In an *in vitro* experiment [8] it is reported that ultrafine AuNPs ($PM_{0.1}$) have been detected in blood and urine three months after exposure. There is a significant amount of literature concerning the possible consequences of inhaling airborne nanoparticles (NPs) into the lung.[9-13] Most of these studies, whether computational or experimental, have been concentrated on the effects of common airborne NPs (carbon[14, 15], silica[16], gold[12, 13], and others[17-19]) on LS monolayer. In these studies, the consequences of airborne NPs inhalation have been investigated in terms of the NPs' size[11], shape[17], surface properties (surface charge, hydrophobicity/hydrophilicity)[20], and concentration.[10] **NP surface charge significantly affects the translocation of the NPs in the surfactant monolayer. For instance, Chen *et al.*[21] reported that an increase in the surface charge of NPs can reduce the translocation of the NPs in the surfactant monolayer. The interaction of NPs with LS** monolayers **at high surface tension can result in the formation of** pores **in LS and the** aggregation of NPs.[10, 11] The presence of NPs has **also** been shown to alter the structural and mechanical properties of LS monolayers, inducing the layer collapse at higher surface tensions.[22] However, when investigating the impact of NPs concentrations on LS monolayer, almost all of the computational studies considered monodisperse NPs, even though the primary sources of airborne NPs (industrial process occurring in urban areas) result in a polydisperse mixture of NPs. Moreover, most simulations studies have overlooked the key role of surfactant peptides.[12, 23] Experimentally, it is challenging to prepare the well-controlled size (high degree of uniformity) NPs and thus polydisperse **samples of** NPs **are used**

[a]*School of Mechanical and Mechatronic Engineering, University of Technology Sydney, 81 Broadway, Ultimo NSW 2007, Australia. E-mail: suvash.saha@uts.edu.au*
[b]*School of Mathematical Sciences, Queensland University of Technology, 2 George Street, GPO Box 2434, Brisbane QLD 4001,*
[c]*School of Chemistry and Biosciences, The University of Bradford, Bradford, BD7 1DP, UK*
Electronic Supplementary Information (ESI) available. See DOI: 10.1039/x0xx00000x

in the determination of Langmuir monolayers' mechanical properties.[24] An experimental study found that the broad size distribution of gold NPs (AuNPs) reduced the stiffness of the lipid layer.[24] In addition, heterogeneity of NP size **may** influence the therapeutic efficacy and translocation ability of the NPs. [25]

The existing literature sufficiently explains the role of surfactant peptides in the LS monolayer[3, 26-28]; however, it is essential to explore the role of SP-B_{1-25} peptides in monolayers exposed to, different concentrations of, NPs. Thus, to gain a **thorough** understanding of the effect of NPs on LS monolayers with SP-B_{1-25} peptide, the impact of polydisperse NP samples requires more significant consideration, particularly for AuNPs. The vast interest of AuNPs in fields like nanomedicine and biotechnology[29, 30], along with the inhalation of bare AuNPs from the environment has raised the question of potential health risk associated with the exposure of AuNPs.[31] For example, gold miners have to face different lung diseases due to exposure to gold dust from their occupational circumstances.[32-34] Recent experimental studies suggested that the inhaled NPs (engineered or environmental) may be responsible for lung-related diseases and AuNPs were detected longer times **after** exposure**, when** compared to other NPs.[8, 35] It has also **been observed** that the detection levels were higher for 5 nm (diameter) sized AuNPs compared to 30 nm (diameter) AuNPs, and that AuNPs with the size <10 nm (diameter) showed higher translocation ability than larger AuNPs.[8] The translocation of AuNPs from the lung to other organs in animal models was investigated by, Yu et *al.*[36], with AuNP aggregation found in the lungs and AuNPs detected 15 days **after** exposure. A study by Takenaka et *al.*[37], used spherical AuNPs with diameters of 5-8 nm (diameter) to investigate the fate of the NPs using experimental methods. It was found that most of the inhaled AuNPs were retained in the lung, and only a meagre amount (0.03-0.06 % of lung concentrations) were transferred from the lung to blood circulation. Bakshi et *al.*[9] and Zhang et *al.*[38] considered AuNPs as a model air pollutant in *in vitro* studies, predicting that the bare AuNPs disrupt routine lung activity, and **that** at high concentration (> 100 µg/mL) **the presence of** AuNPs in the lung could be the reason for the formation of cracks and cavities in the lung monolayer. Moreover, it was hypothesized that the adsorption of AuNPs hinders the ability of the LS to reduce the surface tension of the lung during compression, even in the presence of SP-B.[38] All these experimental studies suggest that the size distribution and concentration of NPs can play an essential role in altering the intrinsic functions of the lungs, as well as the ultimate fate of the inhaled NPs.

In the present study a series of coarse-grained molecular dynamics (CGMD) simulations were performed on the AuNPs LS systems to elucidate the role of peptide and AuNPs, at different AuNP concentrations, **and** on the three states of the LS monolayers. In our previous studies, AuNPs of uniform size (~3 nm diameter) were simulated at different concentrations interacting with LS monolayers at two different surface tensions (relating to the inhalation and exhalation states).[12, 13] However, AuNP **samples** generally exist as **a** polydisperse **mixture**, and such molecules are more to cytotoxic than particles with well-defined size.[39] In previous studies[12, 13] the role of polydispersity and SP-B_{1-25} peptide **was neglected**. Therefore, in th**e present** work, we **intend to** address the **effect** of **the presence of SP**-B_{1-25} in LS monolayers exposed to polydisperse AuNPs. Hence, we modelled LS peptide associated monolayer systems in three different breathing states (I: expanded, II: compressed, and III: re-expanded) at varying levels of AuNP concentration (~0.19 - ~1.53 mol% of AuNPs/lipids). The findings of this study will help to elucidate the molecular mechanism of the interactions among hydrophobic AuNPs, hydrophobic peptide, and other LS components, providing insights into how the inhalation of NPs can contribute to damage to the lungs during different breathing cycles (expansion, compression, and re-expansion) as well as the NPs transportation in LS monolayer with lipoprotein corona formation.

2. Computational methods

Lung surfactant model

The monolayers (Fig. 1) used in the present study as a model for LS membranes consisted of DPPC and POPG PLs, cholesterol, and a segment of surfactant protein B, SP-B_{1-25}. SP-B is a 79 residue long hydrophobic protein with three intramolecular disulfide bridges[40], and is capable of forming a homodimer through another intermolecular disulphide bond. Various SP-B fragments and constructs have been reported[41-43] to attempt to decipher the structure-activity relationship of the full-length peptide, one such peptide SP-B_{1-25} (which incorporates the first 25 residues from N-terminal) was found capable of retaining a substantial level of the biological properties/activities of the full-length SP-B.[44] For example, like SP-B, SP-B_{1-25} enhances the surfactant adsorption process at the air-water interface.[3, 45] Thus, for simplicities sake, we choose to use SP-B_{1-25} in our models. SP-B_{1-25} in humans has the sequence FPIPL PYCWL CRALI KRIQA MIPKG, is a monomer peptide with strong α-helical content, which when surrounded by PLs, is orientated such that the hydrophobic portion of the peptide (residues one to eight) points towards the PL tails.[46] The SP-B_{1-25} molecules were inserted into a lipid bilayer of DPPC:POPG:CHOL using a python script (INSANE[47]). The bilayer was then split into two monolayers, and each monolayer consisted of 1035 lipids and 9 SP-B_{1-25} (with the N-terminus region placed close to lipid head groups), in a ratio of DPPC to POPG to CHOL to SP-B_{1-25} of 70:30:10:1. The monolayers were aligned parallel to the *XY* plane and separated by a ~21 nm layer of 150 mM NaCl aqueous solution (equivalent to ~100000 CG water sites), and ~34 nm of vacuum, with the monolayer lipids, orienting its hydrophilic heads towards the water layer and hydrophobic tails towards the vacuum. Here, we used ~21 nm water layer, such that the diameter of the largest AuNP was significantly less than the distance between the two monolayers, ensuring that any artefacts due to system size were kept to a minimum. Sufficient Na^+ beads above 150 mM NaCl were present to make the system charge neutral.

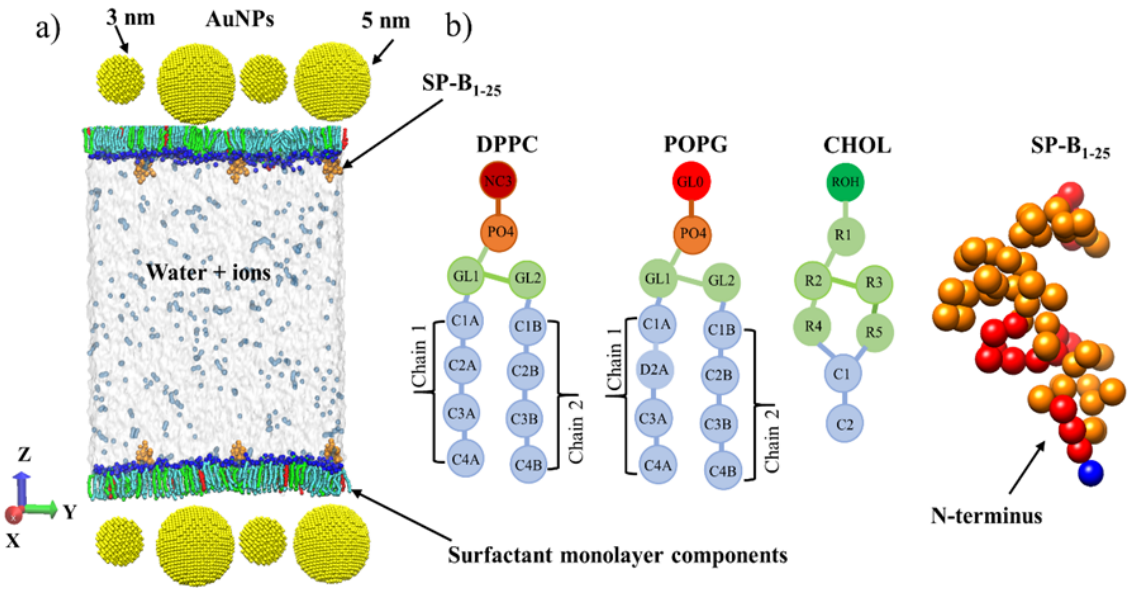

Fig. 1 Model LS monolayer initial structure at the vacuum-water interface in the presence of AuNPs (a) side view of the system with ~1.53 mol% of AuNPs/lipids, PL head group are shown in blue (b) CG structures of surfactant PLs, cholesterol, and SP-B_{1-25}. In SP-B_{1-25}, the charged CG beads are shown in red (positive) and blue (negative), while neutral beads are in coloured orange.

Coarse-grained molecular dynamics simulations

CGMD simulations using the MARTINI force field have been used in most previous simulation studies of LS-NP systems to allow the exploration of long time and length scales.[48, 49] For all simulations in the present study, the MARTINI force field was used to model the surfactant monolayer components, lipids, water, and ions (see Fig. 1). The CG model of SP-B_{1-25} was generated by conversion of an atomistic structure of SP-B_{1-25} (obtained from the protein data bank, PDB ID: 1DFW) via the use of the python script martinize.py from MARTINI website.[50] All-atom structures of two different sizes AuNPs (3 and 5 nm) with a lattice constant of 0.408 nm were obtained from nanoparticle builder of OpenMD[51], which uses Sutton-Chen force field.[52] In contrast to the conventional 4:1 MARTINI mapping, each atom of the AuNPs (887 and 3925 atoms for 3 and 5 nm AuNPs, respectively) was mapped 1:1 to convert the atomistic structures to CG structures. The force field parameters for AuNPs beads were taken from Song et *al.*[53], where each Au bead was assigned as C5-type (hydrophobic) interaction site[53, 54] for spherical CG AuNPs. A weak harmonic potential for bonded interactions[55, 56] was used to establish a connection among the CG AuNPs beads.

All CGMD simulations were performed using a protocol reported previously.[12] For the non-bonded interactions, a cutoff of 1.2 nm was used, with the Coulomb potential smoothly shifted to 0 between 0 and 1.2 nm, and the Lennard-Jones potential was shifted to 0 between 0.9 and 1.2 nm. Periodic boundary conditions were employed in all directions. All the systems were equilibrated for 100 ns and production runs were performed for 3 μs, with a time step of 20 fs used throughout. In all simulations, the temperature coupling was regulated using **velocity rescale** thermostat[57], with the monolayer components (lipids, cholesterol, and SP-B_{1-25}), water and ions, and AuNPs independently coupled to temperature baths at 310 K with time constants of 1 ps.

Simulations were performed at a variety of AuNP concentrations and in different ensembles. **Table 1** summarises the simulations that were performed. First, control systems (state 0) of DPPC:POPG:CHOL:SP-B_{1-25} monolayers were simulated in the absence of AuNPs in the NPγT (constant particle number, pressure, and temperature) ensemble at surface tensions of 0 and 23 mN/m, using Berendsen pressure barostat[57], to reproduce the compressed and expanded states of the surfactant monolayer, respectively. The compressibility was set to 5×10^{-6} bar^{-1} along the *XY* plane and 0 bar^{-1} along the *Z*-axis (such that the size of the simulation cell was fixed along with that dimension). In these control simulations, the area per lipid (APL) obtained after equilibration was 0.470±0.001 and 0.538±0.001 nm^2, for surface tensions of 0 and 23 mN/m, respectively.

The equilibrated control systems were then used as the initial configurations for the simulations of the monolayers in the presence of the AuNPs. The AuNPs were placed in vacuum space, close (< 1 nm, diameter) to the tails of the lipids in equilibrated monolayers. Systems were built at varying concentrations of AuNPs (~0.19, ~0.58, ~0.86, and ~1.53 mol% of AuNPs/lipids). **The concentration modelled ranges from the lowest possible concentration (0.19 mol% of AuNPs/lipids - one 3 nm and one 5 nm AuNP) to the highest practicable concentration (1.53 mol% of AuNPs/lipids - eight 3 nm and eight 5 nm AuNPs) of polydisperse AuNPs for the size of our monolayer system.** For each concentration of AuNPs, we account for polydispersity by having two different sizes (3 and 5 nm) of AuNPs present. All systems contain an equal number of 3 and 5 nm AuNPs. **Due to computational constraints the size of the AuNPs modelled in the present work is at, or slightly**

Table 1. Summary of the systems simulated (666 DPPC, 279 POPG, 90 cholesterol and 9 peptides per monolayer). **Data averaged over 2 or more repeats.**

AuNP concentration (mol %)	No. of AuNPs (state, size) per monolayer	Monolayer State*	Constant		Variable		Pore formation
			Surface tension / mN m^{-1}	APL / nm^2	Surface tension / mN m^{-1}	APL / nm^2	
0	0	0	23			0.538±0.001	No
		0	0			0.470±0.001	No
~0.19	2 (poly.)	I		0.54	26.3±1.6		No
		II		0. 47	21.2±1.3		No
		III	23			0.475±0.006	No
~0.58	6 (poly.)	I		0.54	38.0±0.8		No
		II		0.47	31.2±0.7		No
		III	23			0.440±0.003	No
	6 (mono., 3nm)	I		0.54	22.9±0.4		No
		II		0.47	22.3±2.7		No
	6 (mono., 5nm)	I		0.54	44.2±0.4		No
		II		0.47	37.0±0.3		No
~0.86	9 (poly.)	I		0.54	41.2±2.0		No
		II		0.47	36.1±1.1		No
		III	23			0.429±0.009	No
~1.53	16 (poly.)	I		0.54	47.3± 1.0		Yes
		II		0.47	47.6±0.42		Yes
		III	23			0.426±0.004	Yes

*I: Expanded, II: compressed, and III: re-expanded monolayer systems, poly.: polydisperse (mixed of 3 and 5 nm **diameter** AuNPs), mono.: monodisperse AuNPs

below, the lower end of the size range of AuNPs considered in experimental studies. [9, 37, 38]

To study the effect of dispersity, we have simulated two monodisperse systems - consisting of 3 and 5 nm (diameter) AuNPs at a concentration of ~0.58 mol% of AuNPs/lipids (Table 1). All the systems containing AuNPs were simulated in the canonical (NVT) ensemble at either an APL of 0.54 (state I) or 0.47 (state II) nm^2, corresponding to the expanded and compressed states, respectively. Each system was first equilibrated for a further 100 ns before a 3 μs production run.

After the 3 μs production runs at constant APL, the systems with polydisperse AuNPs at an APL of 0.47 nm^2 were simulated for a further 3 μs in the NPγT ensemble at a surface tension of 23 mN/m (with the compressibility along *XY* plane and *Z*-axis set to 5×10^{-6} and 0 bar^{-1}, respectively). These systems, denoted as state III (re-expanded), were simulated in order to investigate the effects of AuNPs concentrations on LS monolayer breathing cycle, with the monolayers attempting to undergo a re-expansion process.

Analyses were carried out to compute different physical and dynamical properties of LS surfactant components with averages taken from over the last 1 μs of each simulation. **At least two repeat runs were performed for each system, and the analysis of properties averaged over the results of the repeat runs.** All simulations snapshots were taken using the program Visual Molecular Dynamics (VMD).[58] In VMD, a Tcl script[59] (cg_bonds-v5.tcl) was used for rendering CG MARTINI bonds. PLs tails order parameters were determined using do-order-gmx5.py python script.[60] Full methodological details of the analyses are provided in the supporting information, section S1 "Methodological Details of Analyses".

3. Result and discussion

3.1. Effects of SP-B$_{1\text{-}25}$ and AuNPs on LS structure:

3.1.1. Lung surfactant monolayer surface tension:

LS components adsorb at the air-water interface in the form of a monolayer and regulate the surface tension at the interface. Therefore, it is anticipated that the surface tension remains unchanged/constant for the monolayer with a constant surface area until some external factors (e.g. the presence of airborne NPs) alter the surface tension value during breathing. We have shown previously[12, 13] that bare monodisperse AuNPs **increase** the surfactant monolayer surface tension at the interface. In the current study, we consider the effect of AuNPs of different sizes as model NPs to quantify the role of airborne NPs on SP-B$_{1\text{-}25}$ containing LS monolayer in different states (I, II, and III).

To quantify the impact of polydisperse AuNPs over monodisperse AuNPs on monolayer surface tensions, we have measured the surface tensions of the monolayers in the states I, (expanded, APL = 0.54 nm^2) and II (compressed, APL=0.47 nm^2) in the presence of ~0.58 mol% AuNPs/lipids (Fig. 2). In the absence of any AuNPs, the surface tensions of the systems reproduce the physiological surface tensions that occur during the breathing process. However, in the presence of AuNPs, the surface tension increases significantly in both states (Fig. 2, Table 1).

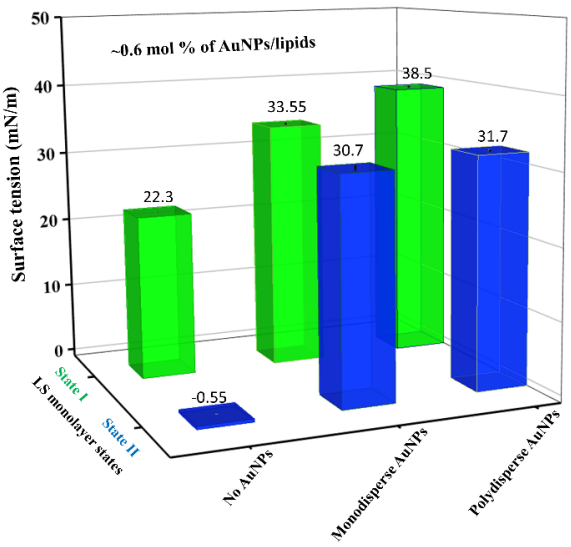

Fig. 2 Comparison between the effects of the monodisperse and polydisperse AuNPs on the surface tensions for the monolayer in states I (APL= 0.54 nm^2) and II (APL=0.47 nm^2) at a concentration of ~0.58 mol% AuNPs/lipids. For the surface tension of monodisperse AuNPs, the average of the surface tensions of systems with 3 and 5 nm diameter AuNPs has been taken. The monolayer interfacial surface tension values of these two states (I and II) without any AuNPs are also presented. **The error bars have been calculated using the standard deviation across repeated runs.**

We observe that polydisperse AuNPs result in a slightly higher surface tension value over averaged monodisperse AuNPs when the monolayer is in state I. However, the effect of polydispersity at ~0.58 mol% AuNPs/lipids appears to be marginal/insignificant on the surface tension of the monolayer in the state II. As the NP concentration increases, so does the surface tension for both states I and II, in agreement with the results of previous studies on monodisperse AuNPs[12] (Table 1). It might be expected that the monolayer will be restored during the re-expansion process, state III, from the compressed state (state II). However, in state III the presence of AuNPs in the LS hindered the ability of the monolayer to return to a surface area of ~0.54 nm^2, even at the lowest AuNP concentration.

The presence of the surfactant peptide, SP-B$_{1\text{-}25}$, in the LS monolayer containing no NPs has only a trivial effect on the monolayer interfacial surface tension, in line with the existing observations from previous studies in case of SP-B in the LS monolayer.[27, 61, 62] We have investigated the effect of the presence of SP-B$_{1\text{-}25}$ on the surface tension values of the monolayer in states I and II with the presence of ~0.86 mol% of monodisperse AuNPs/lipids (Table S1). The simulations predict that the presence of SP-B$_{1\text{-}25}$ marginally reduces the surface tension of the monolayer in state II compared to a monolayer containing no SP-B$_{1\text{-}25}$, but the surface tension slightly increases in the case of the monolayer in state I.

3.1.2 Pore formation in the LS monolayer:

Figure S2 shows representative snapshots of the LS monolayer in state II at different concentrations of AuNPs, both the aggregation of the NPs and the formation of pores are apparent. A higher concentration of NPs results in greater disruption to the LS monolayer and if the NP concentration is sufficiently high pores are formed in the LS. As the concentration of AuNPs in the monolayer increases, the more lipid molecules are adsorbed to the NPs' surface, and this causes pores to be formed. Pores are observed at the AuNPs concentration of ≥1.53 mol% (Fig. S2d) for the polydisperse AuNPs (3 and 5 nm), whereas no pores in the monolayer are formed for ≤ 1.56 mol% of AuNPs/lipids for monodisperse AuNPs with diameter of 3 nm[12], this difference is because of the total surface area of AuNPs is greater in the former than in the latter. Pores are also formed in the monolayer in other two states (I and III) (data not shown for brevity), which implies that pores formation does not depend on the monolayer breathing conditions/states. The formation of pores in the LS monolayer due to the presence of sufficient AuNP concentration agrees with an experimental study that reports cracks in the monolayer observed as AuNPs concentration is increased.[38] **Therefore, we believe that the formation of pores in the monolayer due to NP adsorption is representative of the true behaviour of the modelled systems.** The formation of persistent pores in the LS monolayer can be a cause of serious health problems, including the hindrance of normal gas exchange process inside the alveoli and surfactant monolayer associated water level elevation.[63, 64] As a result, the required oxygen cannot reach into the bloodstream and one could develop acute respiratory distress syndrome. Lipids adsorb to the NPs' hydrophobic surface, which affects the packing of lipids in the monolayer. In the present study, the diameter of the AuNPs modelled (3 and 5 nm) is greater than the monolayer thickness (~2 nm). As a result, the adsorption of the lipids on AuNP surface results in the prevention of the exposure of the bare surface of the AuNPs to the vacuum and/or water phases. The same observation was previously found in a simulated study for the environmental hydrophobic carbon NP surface exposed to air.[65] **Radial distribution functions (RDF) of surfactant lipids (DPPC, POPG, CHOL and SP-B$_{1\text{-}25}$) to AuNPs 3 nm (Fig. S3a) and 5 nm (Fig. S3b) represent the preference of the surfactant lipids to the AuNPs surface. In both cases (3 and 5 nm), the cholesterol molecule has the greater interaction to AuNP than other two phospholipids (DPPC, POPG and SP-B$_{1\text{-}25}$). The high preference of cholesterol molecules to AuNPs arises due to the hydrophobic-hydrophobic interaction.**

In the present investigation, the simulations predict the aggregation of polydisperse AuNPs (vide infra), and the formation of a reverse micellar structure around of the AuNPs is observed (Fig. S4). The formation of the reverse micelles in the monolayers occurs as a result of some of the PLs orientating themselves with their headgroups directed away from the NP surface.

In our previous study, we found an aggregation of the AuNPs in the monolayer[12], and prior CGMD simulation studies have predicted that the adsorbed lipids form reverse micelles around the NPs, which can influence the aggregation of NPs within LS monolayers. [66]

3.1.3 Lung surfactant monolayer components' density profiles:

To measure the effects of surfactant peptide (SP-B_{1-25}) and polydispersity of AuNPs on the surfactant lipids density profiles,

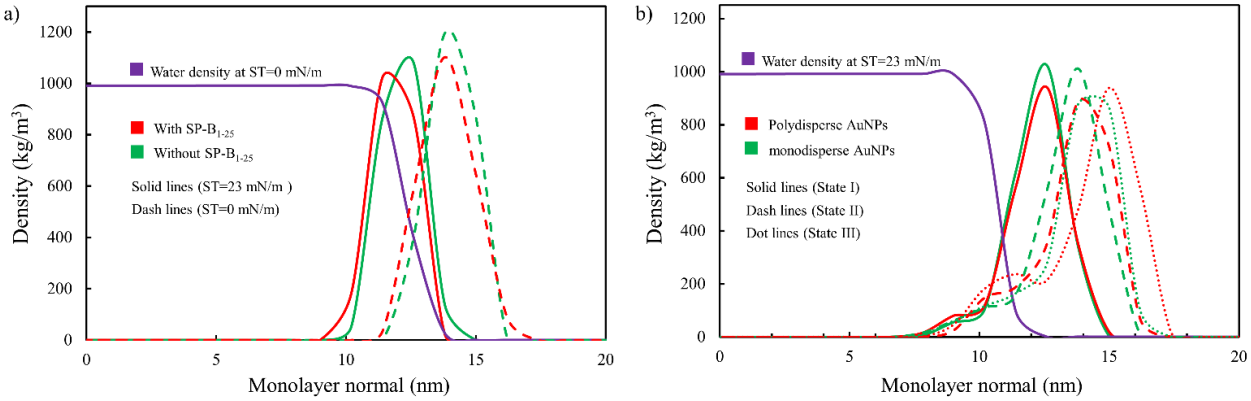

Fig. 3 (a) Lipid density profiles of LS monolayers in absence of AuNPs, for monolayers free of SP-B_{1-25} (green) and with SP-B_{1-25} present (red) at surface tensions (ST) of 23 (solid lines) and 0 mN/m (dashed lines). (b) Lipid density profiles for LS monolayers in the presence of AuNPs, for systems with monodisperse (green) and polydisperse (red) samples of AuNPs at an exemplar concentration of ~0.86 mol% of AuNPs/lipids for the monolayer in states I (solid lines), II (dashed lines), and III (red-dotted lines). Water density profiles (purple) were computed at surface tensions (a) 0 and (b) 23 mN/m.

we have computed the lipid (DPPC, POPG, CHOL) density profiles between the systems with and without SP-B_{1-25} (Fig. 3a) as well as between the systems with monodisperse and polydisperse AuNPs (Fig. 3b) at a concentration of ~0.86 mol% of AuNPs. Comparison of the peak heights of the lipid density profiles of the monolayers containing SP-B_{1-25} with monolayers where SP-B_{1-25} is absent indicates that the former has a slightly lower the peak height than the latter at both surface tensions (Fig. 3a). The result indicates that the surfactant monolayer-associated peptides participate in decreasing lipid density profiles i.e., fluidizing the monolayer components, which is in reasonable agreement with previous in silico[3] and in vitro[67] studies. At an AuNPs concentration of 0.86 mol%, there is a small reduction in the peak height of the lipid density profiles for the polydisperse systems over the monodisperse systems in states I and II (Fig. 3b). For the monolayers in state III (at a concentration of 0.86 mol% of AuNPs/lipids), the peak height of the density profiles of the lipids are slightly higher for the polydisperse system than the monodisperse one (Fig. 3b). During the simulation of the monolayers (all states) exposed to NPs (monodisperse/polydisperse), the NPs have lipids adsorbed to their surface, which induces long tails in the density profiles (Fig. 3b) towards the water layer and thus decreases the height of the peak in the density profiles of the lipids from the control values (peak height of density profiles of lipids in the monolayer without NPs). The density profiles of the individual components of the surfactant monolayer (DPPC:POPG:CHOL:SP-B_{1-25}) and water have been plotted in Fig. S5 (insets: cholesterol and SP-B_{1-25} densities for clarity) for the systems with the polydisperse AuNPs. The density profiles have been calculated for the monolayer in states I (Fig. S5a) and II (Fig. S5b). The AuNPs disrupt the orientation of the lipids, and thus the height of the peak in the density profile of each component of the LS monolayer is reduced compared to the control simulations. The density profile curves in Fig. S5 show that at the lowest concentrations AuNPs (~0.19-0.86 mol% of AuNPs/lipids) there is a negligible change in the LS density profiles, whereas the highest concentration ~1.53 mol% of AuNPs/lipids substantially changes the density profiles for each LS components.

The concentration effects of AuNPs are more significant in the state II systems than in the state I systems because lipids are more densely arranged in the monolayers in the state II than in the state I. The density profiles of cholesterol and SP-B_{1-25} follow a similar trend to the PLs density profiles for all concentrations of polydisperse AuNPs (Fig. S5 insets).

3.1.4 Lung surfactant monolayer lipid ordering:

Lipid order parameters provide information about the phase of the monolayer and fluctuations in the order parameter values can indicate that lipids are in a phase transition state. The lipids in the LC phase of a monolayer are highly ordered and exhibit high values of the order parameter unlike the lipids in a LE phase. However, the presence of NPs has a substantial impact on the lipid order parameter values. The order parameter of lipid tails decreased for all three states (Fig. 4 and Fig. S6), for both chains in the presence of the NPs. As the AuNP concentration increased, the order parameters decreased. The phenomena of lipid disordering is more noticeable in lipid chain 1 (Fig. 4a, c and Fig. S6a) than chain 2 (Fig. 4b, d and Fig. S6b). The results, as shown in Fig. 4, indicate that the AuNPs disturb the lipids' systematic arrangement in the monolayer and the high concentration of the NPs substantially changes the physiological ordering of the lipids in the monolayers. The presence of SP-B_{1-25} in the monolayer slightly decreases the ordering of both phospholipids (DPPC, POPG) tail beads (Fig. S7a, b) compared to a system without any surfactant proteins present. On the other hand, only marginal differences in order parameters for both lipid species were observed in case of polydispersed versus monodispersed AuNPs at a concentration ~0.58 mol% of AuNPs/lipids in the monolayer in state II (Fig. S7c, d).

3.1.5 Lung surfactant monolayer folding, SP-B_{1-25} cluster formation, and aggregation of AuNPs:

A CGMD study by Duncan et *al.*[3] revealed that LS monolayer folding occurs when either the fold nucleates about a defect.

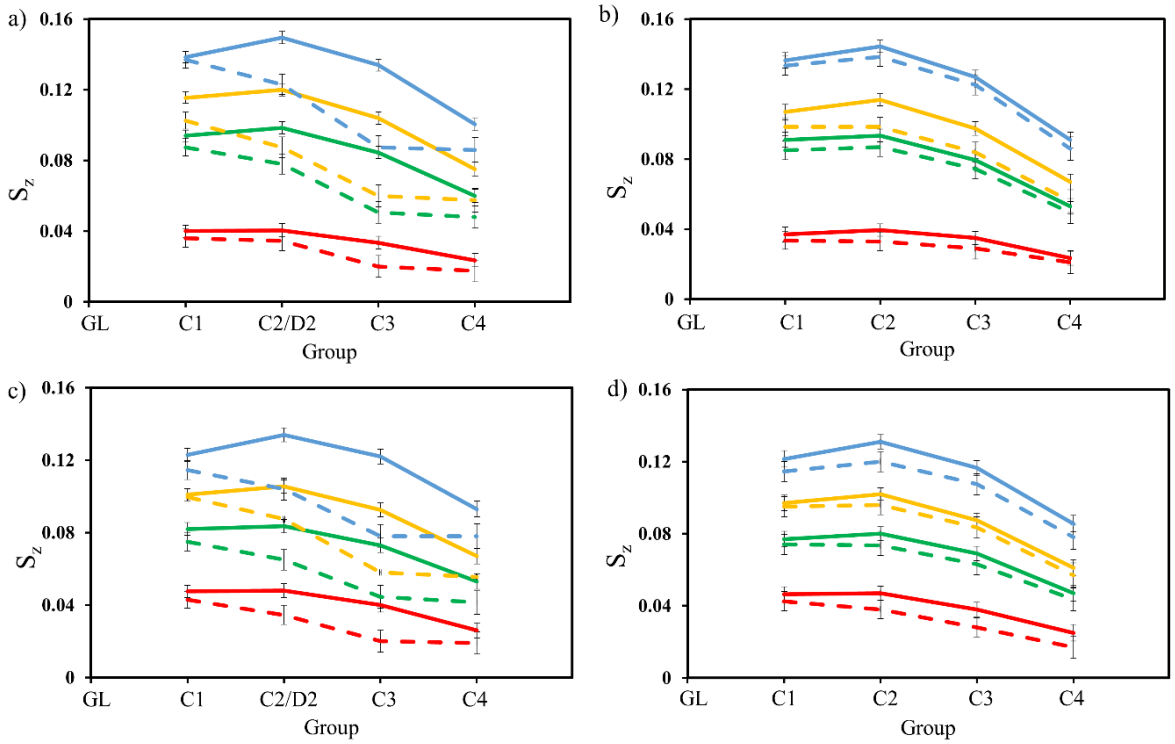

Fig. 4 The effect of AuNPs concentrations on DPPC (solid lines) and POPG (dash lines) lipid tail order parameters, chain 1 (*sn*-1) in (a, c) and chain 2 (*sn*-2) in (b, d) of the monolayer in states I (a, b) and II (c, d). The ~0.19, ~0.58, ~0.86, and ~1.53 mol% concentrations of AuNPs/lipids are shown by the blue, yellow, green, and red lines respectively. **The error bars have been calculated using the standard deviation across at least two repeat runs.**

owing to the perturbation of the monolayer peptide SP-$B_{1\text{-}25}$ or by the undulations of the monolayer. Our results also indicate that SP-$B_{1\text{-}25}$ aggregates in the monolayer forming clusters of peptides, with a fold then nucleating at the site of this cluster (Fig. 5) in the NP free monolayer. A finding that agrees with the claims made by Duncan et *al.*[3] In the monolayer, the positively charged peptide SP-$B_{1\text{-}25}$ (5 positively charged residues) is found to adhere with the heads of the surfactant PLs (Fig. 5c). The preference of SP-$B_{1\text{-}25}$ to the PLs head groups is because the surfactant PLs contain anionic lipid POPG (with a negative charge in the headgroup). This lends support to the previous in vitro findings.[44, 68] These electrostatic interactions between the anionic POPG and cationic SP-$B_{1\text{-}25}$ have been proposed to play a significant role in lamellar bodies (LB) formation, protein surface activities and aggregation in the LS monolayer.[69]

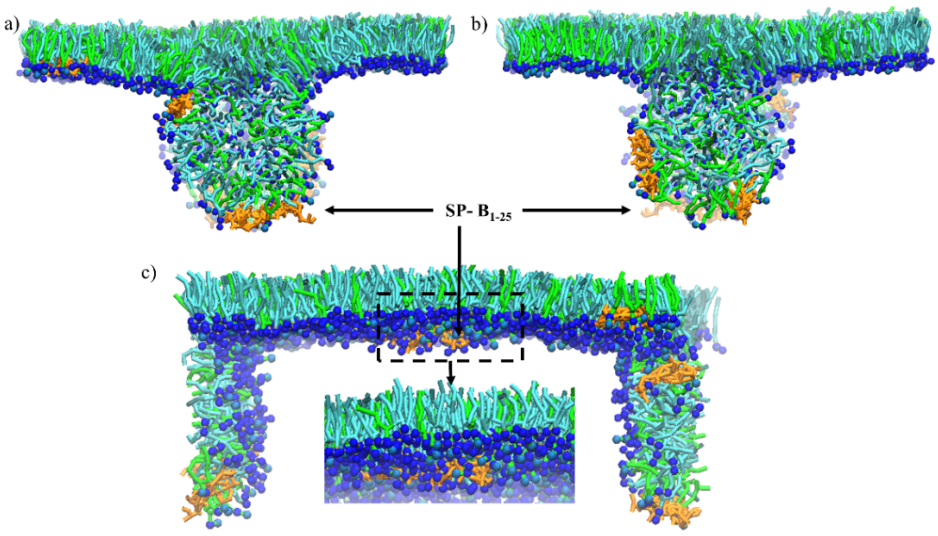

Fig. 5 Monolayer folding associated with the SP-B_{1-25} aggregation, for a monolayer at a surface tension of 0 mN/m: (a-b) two side views of the beginning of monolayer to bilayer transformation, and (c) snapshot showing the close correspondence of SP-B_{1-25} with the head groups of PLs. All the snapshots were taken during monolayer compression at surface tension 0 mN/m of the DPPC:POPG:CHOL:SP-B_{1-25} system, in the absence of NPs.

Experimentally, it has been demonstrated that LS monolayer compression has less influence in the SP-B clustering process, but the protein concentration in the monolayer is key in determining the size and number of protein clusters in the monolayer.[70] To investigate the aggregation behaviour of SP-B_{1-25}, we performed a cluster analysis of the protein segments throughout the simulation (Fig S8a). Two or more peptides were assigned to the same cluster if the distance between them was ≤ 1.2 nm. Initially, the SP-B_{1-25} molecules are well distributed in the monolayer, but by 2 μs every peptide is part of a cluster of at least two molecules. A representative snapshot (Fig. S8b) and 2D map of the peptide density (Fig. S8c) confirm this aggregation behaviour and show how the peptide is distributed in the equilibrated **(at surface tension 0 mN/m)** monolayer.

While SP-B_{1-25} aggregates even in the absence of NPs, the adsorption of NPs into the LS monolayer sharply increases the aggregation of the peptide. A plot showing the formation of clusters of SP-B_{1-25} in the presence of AuNPs is given for an exemplar system (state II, 0.19 mol% of AuNPs) in Fig. 6.

The presence of the AuNPs increases the propensity of the peptide to aggregate in a monolayer, with the number of peptides present in the largest cluster higher than in the absence of any AuNPs (Fig. S8) even for systems with the lowest AuNP concentration (Fig. 6 and S9). Both the number of clusters and the number of peptides in the largest cluster stabilize more quickly in the presence of the hydrophobic AuNPs in state II (Fig. 6) than in the case of state I (Fig S9) or in the monolayer in the absence of AuNPs (Fig. S8), indicating that the clusters are apparently more stable for monolayers with a lower surface area. In addition, the number of peptide clusters predicted in the monolayers in state II remain nearly unchanged during the expansion process of the monolayers in state III (Fig. S10). We hypothesise that the increased aggregation of SP-B_{1-25} in the presence of AuNPs is driven by a hydrophobic interaction between the two species. Ultimately, the clustering of the proteins in the LS monolayer coupled with the hydrophobic AuNPs presence in the monolayer may lead to lipoprotein corona formation on the NPs surface (Fig. S11).

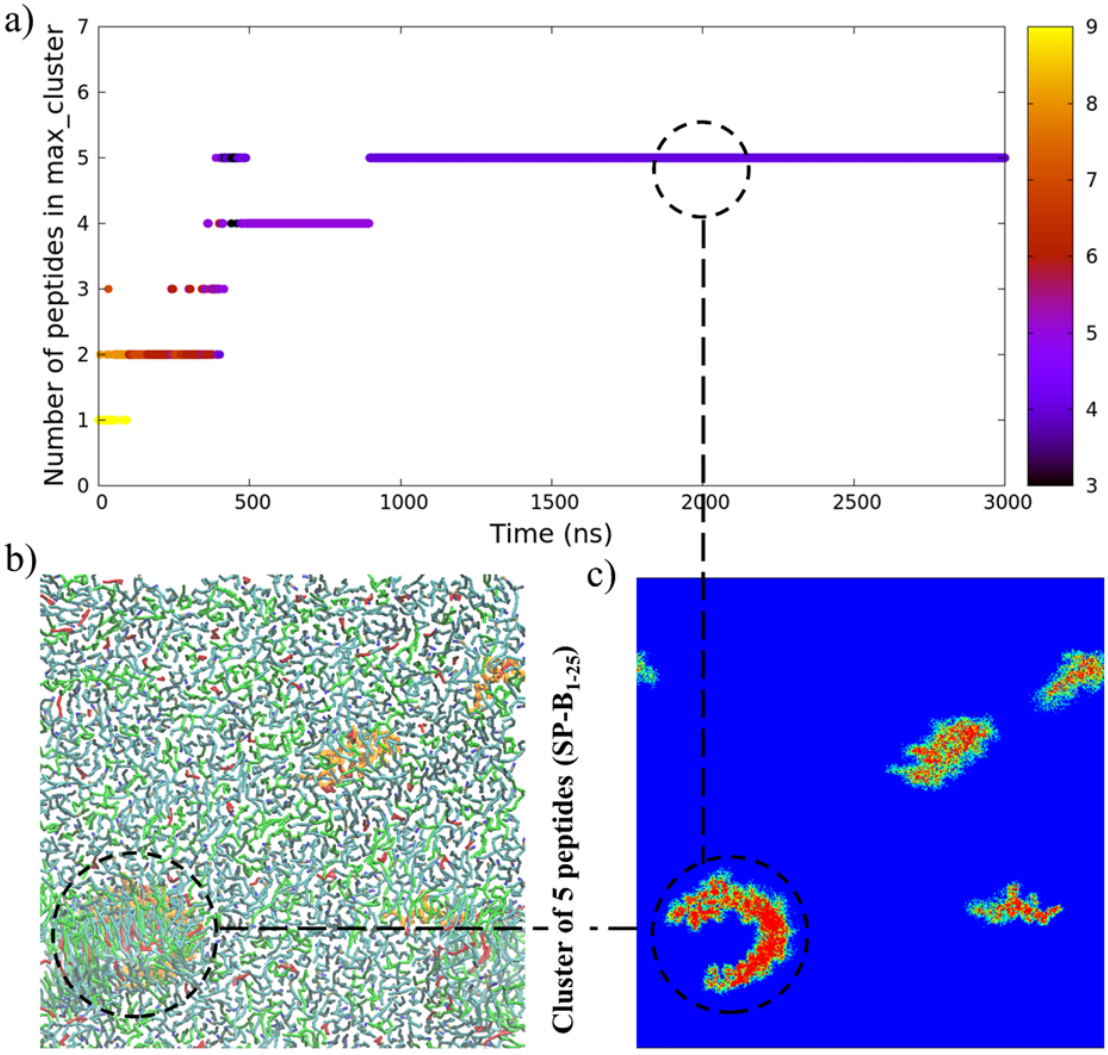

Fig. 6 (a) Cluster size analysis of surfactant peptide B (SP-B_{1-25}) in state II (APL of ~0.47 nm^2) with a AuNP concentration of ~0.19 mol% of AuNPs/lipids, simulation time is presented along X-axis, the number of SP-B_{1-25} in the largest cluster is presented along Y-axis, and the number of clusters is presented along Z-axis, (b) visualization of SP-B_{1-25} clustering in the surfactant monolayer (top view), and (c) SP-B_{1-25} number density map after 2 µs of simulation.

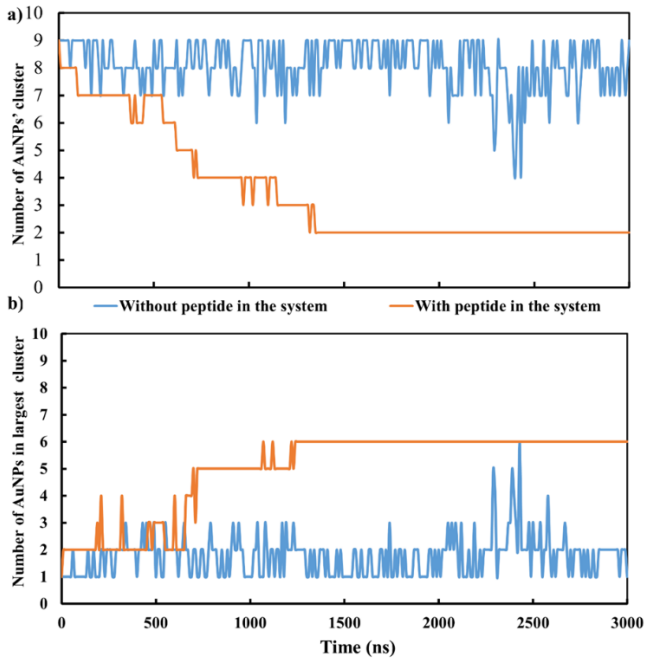

Fig. 7 Effects of SP-B_{1-25} on AuNP (~0.9 mol% of AuNPs/lipids) aggregation in LS monolayer in state II, in the presence (orange) and absence (blue) of SP-B_{1-25}. The analyses have been performed over the full 3 µs of simulation.

We have considered two systems to measure the role of SP-B_{1-25} in AuNP clustering, one with and another one without SP-B_{1-25}, where each system contains 3 nm-sized monodisperse AuNPs at a concentration of ~0.9 mol% of AuNPs/lipids and each monolayer is in state II. In the presence of hydrophobic surfactant peptide SP-B_{1-25}, the number of AuNPs clusters is decreased, and the number of AuNPs in the largest cluster is increased (Fig. 7). Therefore, we conclude that AuNPs and the SP-B_{1-25} peptide have a co-operative effect mutually increasing the propensity of both to aggregate.

3.2 Effects of SP-B_{1-25} and AuNPs on LS PLs diffusion:

To investigate the effect of the presence of SP-B_{1-25} on the lateral mobility of the PLs the 2-dimensional (2D) lateral mean-square displacement (MSD) has been calculated for systems with and without SP-B_{1-25} (MSD calculation details have been provided in the ESI). In the presence of SP-B_{1-25}, the diffusion of the PLs in the **compressed** monolayer is **slightly** increased (Fig. S12). This is because the hydrophobic peptide, SP-B_{1-25}, fluidizes the LS monolayer[3] and thus the PL MSD is greater in the monolayer with surfactant peptide over without peptide system.

We have measured the PLs' 2D MSD (Fig. S13 for state I) and lateral diffusion coefficients (Fig. S14) in all the three states (I, II, and III) of the surfactant monolayer at four different concentrations of AuNPs (~0.19, ~0.58, ~0.86, and ~1.53 mol% of AuNPs/lipids). The 2D MSD, and thus the lateral diffusion coefficients, of PLs in the monolayer significantly decrease with the increasing concentration of AuNPs present in the monolayer. We have observed that a drastic fall in the PL diffusion coefficient with the increase of AuNPs concentration from 0.19 to 0.58 mol% for monolayers in states II and III. We propose that this is because of the adsorption of PLs to the NPs' surface and subsequent formation of clusters of NPs (vide supra) hinders the ability of the PLs to diffuse. The PLs adsorption on the NP surfaces and subsequent formation of nano-clusters is promoted due to the decrease of the PLs free space in the monolayer with an increased volume of AuNPs.

The diffusion of PLs in the LS monolayers (state II) exposed to polydisperse AuNPs is lower compared to the monodisperse AuNPs **(3 and 5 nm)** at a concentration of ~0.58 mol% of AuNPs/lipids (Fig. S15). This result is due to the fact that the total AuNP surface area is greater for the polydisperse **and monodisperse AuNPs (5 nm)** systems than the monodisperse system **with 3 nm AuNPs**, and so, more lipids are able to adsorb to the AuNPs surface, thus reducing the rate of diffusion of PLs.

Conclusions

The adsorption of polydisperse samples of AuNPs to LS monolayer containing a hydrophobic peptide have been modelled for three different breathing cycles using CGMD simulations. The presence of the peptide (SP-B_{1-25}) and NPs in the LS monolayer mutually promote the aggregation of both species via hydrophobic interaction. In addition, the hydrophobic properties of the NPs, SP-B_{1-25}, and the tails of the surfactant lipids induce an interaction between the surfactant molecules and the NPs, which could lead to lipoprotein corona formation. As a result, the biophysical functions of the LS monolayer in expanded, compressed and re-expanded states could be hampered. It is found that despite an attempted re-expansion process LS monolayers which have NPs embedded within them are unable to achieve a surface area similar to NP free monolayers. Furthermore, the AuNP concentration markedly affects the diffusion of the PLs process because of the PLs adsorption to the NPs' surface. The current study has identified that the levels of NP polydispersity considered in this study have a significant role, but limited effect on the behaviour of LS monolayers. The insights gained from this study will be of assistance to understand the NPs contribution on monolayer pore formation, a contributor to lung diseases. The findings of these model simulations will assist the nanotechnologists, biophysicist, and pharmacist to model nanomedicine for lung area in future.

Conflicts of interest

There are no conflicts to declare.

Acknowledgements

This work was completed with the support of University of Technology Sydney (UTS) FEIT Research Scholarship, UTS IRS (S.I.H.). The computational facilities were provided by the UTS eResearch High-Performance Computer Cluster and NCI Australia.

References

1. J. Goerke, *Biochimica et Biophysica Acta (BBA) - Molecular Basis of Disease*, 1998, **1408**, 79-89.
2. J. Pérez-Gil, *Biochimica et Biophysica Acta (BBA) - Biomembranes*, 2008, **1778**, 1676-1695.
3. S. L. Duncan and R. G. Larson, *Biochimica et Biophysica Acta (BBA) - Biomembranes*, 2010, **1798**, 1632-1650.
4. B. Pastrana-Rios, C. R. Flach, J. W. Brauner, A. J. Mautone and R. Mendelsohn, *Biochemistry-Us*, 1994, **33**, 5121-5127.
5. S. Baoukina and D. P. Tieleman, *Biochimica et Biophysica Acta (BBA) - Biomembranes*, 2016, **1858**, 2431-2440.
6. H. Zhang, Y. E. Wang, Q. Fan and Y. Y. Zuo, *Langmuir*, 2011, **27**, 8351-8358.
7. M. B. Rice, P. L. Ljungman, E. H. Wilker, K. S. Dorans, D. R. Gold, J. Schwartz, P. Koutrakis, G. R. Washko, G. T. O'Connor and M. A. Mittleman, *American journal of respiratory and critical care medicine*, 2015, **191**, 656-664.
8. M. R. Miller, J. B. Raftis, J. P. Langrish, S. G. McLean, P. Samutrtai, S. P. Connell, S. Wilson, A. T. Vesey, P. H. B. Fokkens, A. J. F. Boere, P. Krystek, C. J. Campbell, P. W. F. Hadoke, K. Donaldson, F. R. Cassee, D. E. Newby, R. Duffin and N. L. Mills, *ACS Nano*, 2017, **11**, 4542-4552.
9. M. S. Bakshi, L. Zhao, R. Smith, F. Possmayer and N. O. Petersen, *Biophysical Journal*, 2008, **94**, 855-868.
10. N. Nisoh, M. Karttunen, L. Monticelli and J. Wong-ekkabut, *RSC Advances*, 2015, **5**, 11676-11685.
11. C.-c. Chiu, W. Shinoda, R. H. DeVane and S. O. Nielsen, *Soft Matter*, 2012, **8**, 9610-9616.
12. S. I. Hossain, N. S. Gandhi, Z. E. Hughes, Y. T. Gu and S. C. Saha, *Biochimica et Biophysica Acta (BBA) - Biomembranes*, 2019, **1861**, 1458-1467.
13. S. I. Hossain, N. S. Gandhi, Z. E. Hughes and S. C. Saha, *MRS Advances*, 2019, **4**, 1177-1185.
14. T. Yue, Y. Xu, S. Li, Z. Luo, X. Zhang and F. Huang, *RSC Advances*, 2017, **7**, 20851-20864.
15. S. Choe, R. Chang, J. Jeon and A. Violi, *Biophysical Journal*, 2008, **95**, 4102-4114.
16. X. Ye, C. Hao, J. Yang and R. Sun, *Colloids and Surfaces B: Biointerfaces*, 2018, **172**, 480-486.
17. X. Lin, Y. Y. Zuo and N. Gu, *Science China Materials*, 2015, **58**, 28-37.
18. G. Hu, B. Jiao, X. Shi, R. P. Valle, Q. Fan and Y. Y. Zuo, *ACS Nano*, 2013, **7**, 10525-10533.
19. K. Yue, X. Sun, J. Tang, Y. Wei and X. Zhang, *International journal of molecular sciences*, 2019, **20**, 3281.
20. M. Ratoi, P. H. M. Hoet, A. Crossley and P. Dobson, *RSC Advances*, 2014, **4**, 20573-20581.
21. P. Chen, Z. Zhang, N. Gu and M. Ji, *Molecular Simulation*, 2018, **44**, 85-93.
22. J. Barnoud, L. Urbini and L. Monticelli, *Journal of The Royal Society Interface*, 2015, **12**.
23. J. Löndahl, W. Möller, J. H. Pagels, W. G. Kreyling, E. Swietlicki and O. Schmid, *Journal of aerosol medicine and pulmonary drug delivery*, 2014, **27**, 229-254.
24. S. S. You, R. Rashkov, P. Kanjanaboos, I. Calderon, M. Meron, H. M. Jaeger and B. Lin, *Langmuir*, 2013, **29**, 11751-11757.
25. I. M. Adjei, C. Peetla and V. Labhasetwar, *Nanomedicine*, 2014, **9**, 267-278.
26. A. Chakraborty, E. Hui, A. J. Waring and P. Dhar, *Biochimica et Biophysica Acta (BBA)-Biomembranes*, 2016, **1858**, 904-912.
27. S. Baoukina and D. P. Tieleman, *Biophysical Journal*, 2011, **100**, 1678-1687.
28. E. J. A. Veldhuizen, A. J. Waring, F. J. Walther, J. J. Batenburg, L. M. G. van Golde and H. P. Haagsman, *Biophysical Journal*, 2000, **79**, 377-384.
29. E. C. Dreaden, A. M. Alkilany, X. Huang, C. J. Murphy and M. A. El-Sayed, *Chem Soc Rev*, 2012, **41**, 2740-2779.
30. R. Gupta, N. Kashyap and B. Rai, *Physical Chemistry Chemical Physics*, 2017, **19**, 7537-7545.
31. I. Fratoddi, I. Venditti, C. Cametti and M. V. Russo, *Nano Research*, 2015, **8**, 1771-1799.
32. F. J. Wiles and M. H. Faure, *Inhaled particles*, 1975, **4 Pt 2**, 727-735.
33. E. Ayaaba, Y. Li, J. Yuan and C. Ni, *International Journal of Environmental Research and Public Health*, 2017, **14**, 337.
34. A. B. G. Lansdown, *Critical reviews in toxicology*, 2018, **48**, 596-614.
35. J. H. Sung, J. H. Ji, J. D. Park, M. Y. Song, K. S. Song, H. R. Ryu, J. U. Yoon, K. S. Jeon, J. Jeong, B. S. Han, Y. H. Chung, H. K. Chang, J. H. Lee, D. W. Kim, B. J. Kelman and I. J. Yu, *Particle and fibre toxicology*, 2011, **8**, 16-16.
36. L. E. Yu, L.-Y. Lanry Yung, C.-N. Ong, Y.-L. Tan, K. Suresh Balasubramaniam, D. Hartono, G. Shui, M. R. Wenk and W.-Y. Ong, *Nanotoxicology*, 2007, **1**, 235-242.
37. S. Takenaka, E. Karg, W. Kreyling, B. Lentner, W. Möller, M. Behnke-Semmler, L. Jennen, A. Walch, B. Michalke and P. Schramel, *Inhalation toxicology*, 2006, **18**, 733-740.
38. K. Zhang, L. Liu, T. Bai and Z. Guo, *Journal of biomedical nanotechnology*, 2018, **14**, 526-535.
39. D. Huang, H. Zhou, H. Liu and J. Gao, *Dalton Transactions*, 2015, **44**, 17911-17915.
40. J. Johansson, T. Curstedt and H. Jornvall, *Biochemistry-Us*, 1991, **30**, 6917-6921.
41. M. Sarker, A. J. Waring, F. J. Walther, K. M. Keough and V. Booth, *Biochemistry-Us*, 2007, **46**, 11047-11056.
42. M. A. Ryan, X. Qi, A. G. Serrano, M. Ikegami, J. Perez-Gil, J. Johansson and T. E. Weaver, *Biochemistry-Us*, 2005, **44**, 861-872.
43. N. Biswas, S. Shanmukh, A. J. Waring, F. Walther, Z. Wang, Y. Chang, R. H. Notter and R. A. Dluhy, *Biophysical Chemistry*, 2005, **113**, 223-232.
44. M. Longo, A. Bisagno, J. Zasadzinski, R. Bruni and A. Waring, *Science*, 1993, **261**, 453-456.
45. V. Schram and S. B. Hall, *Biophysical journal*, 2001, **81**, 1536-1546.
46. L. M. Gordon, S. Horvath, M. L. Longo, J. A. Zasadzinski, H. W. Taeusch, K. Faull, C. Leung and A. J. Waring, *Protein Science*, 1996, **5**, 1662-1675.
47. T. A. Wassenaar, H. I. Ingolfsson, R. A. Bockmann, D. P. Tieleman and S. J. Marrink, *J Chem Theory Comput*, 2015, **11**, 2144-2155.
48. S. J. Marrink, H. J. Risselada, S. Yefimov, D. P. Tieleman and A. H. de Vries, *Journal of Physical Chemistry B*, 2007, **111**, 7812-7824.
49. Z.-J. Wang and M. Deserno, *The Journal of Physical Chemistry B*, 2010, **114**, 11207-11220.
50. L. Monticelli, S. K. Kandasamy, X. Periole, R. G. Larson, D. P. Tieleman and S.-J. Marrink, *J Chem Theory Comput*, 2008, **4**, 819-834.
51. Gezelter, J. D.; Kuang, S.; Marr, J.; Stocker, K.; Li, C.; Vardeman, C. F.; Lin, T.; Fennell, C. J.; Sun, X.; Daily, K.; Zheng, Y. OpenMD, an Open Source Engine for Molecular Dynamics; University of Notre Dame: Notre Dame, IN., http://openmd.org/, (accessed April 2017).
52. A. Sutton and J. Chen, *Philosophical Magazine Letters*, 1990, **61**, 139-146.
53. B. Song, H. Yuan, C. J. Jameson and S. Murad, *Molecular Physics*, 2011, **109**, 1511-1526.
54. J. Lin, H. Zhang, Z. Chen and Y. Zheng, *ACS Nano*, 2010, **4**, 5421-5429.
55. O. Lopez-Acevedo, J. Akola, R. L. Whetten, H. Grönbeck and H. Häkkinen, *The Journal of Physical Chemistry C*, 2009, **113**, 5035-5038.
56. S. Salassi, F. Simonelli, D. Bochicchio, R. Ferrando and G. Rossi, *The Journal of Physical Chemistry C*, 2017, DOI: 10.1021/acs.jpcc.6b12148.
57. H. J. C. Berendsen, J. P. M. Postma, W. F. v. Gunsteren, A. DiNola and J. R. Haak, *The Journal of Chemical Physics*, 1984, **81**, 3684-3690.
58. W. Humphrey, A. Dalke and K. Schulten, *Journal of Molecular Graphics*, 1996, **14**, 33-38.
59. Martini Coarse Grain Forcefield for Biomolecules, http://www.cgmartini.nl/index.php/tools2/visualization, (accessed January 2019).
60. Martini Coarse Grain Forcefield for Biomolecules, http://www.cgmartini.nl/index.php/downloads/tools/229-do-order, (accessed on Jaanuary 2019).
61. E. J. A. Veldhuizen and H. P. Haagsman, *Biochimica et Biophysica Acta (BBA) - Biomembranes*, 2000, **1467**, 255-270.
62. S. Hawgood, M. Derrick and F. Poulain, *Biochimica et Biophysica Acta (BBA)-Molecular Basis of Disease*, 1998, **1408**, 150-160.
63. Y. Xu, S. Li, Z. Luo, H. Ren, X. Zhang, F. Huang, Y. Y. Zuo and T. Yue, *Langmuir*, 2018, **34**, 9054-9063.
64. Q. Hu, B. Jiao, X. Shi, R. P. Valle, Y. Y. Zuo and G. Hu, *Nanoscale*, 2015, **7**, 18025-18029.
65. Z. Luo, S. Li, Y. Xu, Z. Yan, F. Huang and T. Yue, *Environmental Science: Nano*, 2018, **5**, 1921-1932.
66. T. Yue, Y. Xu, S. Li, X. Zhang and F. Huang, *Physical Chemistry Chemical Physics*, 2016, **18**, 18923-18933.
67. S. Krol, M. Ross, M. Sieber, S. Künneke, H.-J. Galla and A. Janshoff, *Biophysical Journal*, 2000, **79**, 904-918.
68. J. E. Baatz, B. Elledge and J. A. Whitsett, *Biochemistry-Us*, 1990, **29**, 6714-6720.
69. A. G. Serrano and J. Pérez-Gil, *Chemistry and Physics of Lipids*, 2006, **141**, 105-118.
70. A. Cruz, L. Vázquez, M. Vélez and J. Pérez-Gil, *Biophysical journal*, 2004, **86**, 308-320.